OSIRIS

Optical, Spectroscopic, and Infrared Remote Imaging System

OSIRIS camera distortion and boresight correction

RO-RIS-MPAE-TN-081

Issue: 2

Revision: -

17 December 2021

Prepared by:

G. Kovacs

Approval Sheet

Gabor Kovacs Digitálisan aláírta: Gabor Kovacs
Dátum: 2021.12.20 14:37:10 +01'00'

Prepared by: G. Kovacs (signature/date)

Digitally signed by Holger Sierks
Date: 2021.12.20 15:44:01 +01'00'

Approved by: H. Sierks (signature/date)

Document Change Record

Iss./Rev.	Date / Author	Pages affected	Description
D / -	11/05/2015 Kovacs	all	first draft
1 / -	29/06/2015 Kovacs	all	first issue
1 / a	22/2/2017 Tubiana	Sec. 5	Section added Inserted Table of Content, List of Tables
1 / b	13/02/2018 Güttler/Kovacs	Sect. 3.3	Added parameter validation Minor (format and wording) changes throughout
1 / c	5 Nov 2019 Kovacs/Tubiana	Sect. 2, 4, 5	Modified distortion centre, added filter effect on distortion and pointing
1 / d	10 Jul 2020 Tubiana	all	Updated WAC geometric distortion correction; Updated the shift of the boresight position due to the filters in the optical path; Added the shift of the boresight position due to temperature variations. Added Sec. 6. Added Appendix A.
2 / -	17 Dec 2021 Güttler/Kovacs	all	- updated general description and distortion equations (mostly Sect. 2) - introduced level 2 iFoV (Sect. 7) - new resampling algorithm (Sect. 8)

Table of contents

1 General aspects ... 6
1.1 Scope ... 6
1.2 Introduction ... 6
1.3 Reference Documents ... 6
1.4 Acronyms and Abbreviations ... 6
2 Correction of the Image ... 7
3 Distortion Correction ... 9
3.1 Distortion Correction Parameters ... 9
3.2 Distortion Correction Reference Point ... 9
3.3 Distortion Correction Parameters Validation ... 10
3.3.1 Calculation Method ... 11
3.3.2 Validation Results ... 11
4 Effect of the Band-Pass Filters on Boresight Position ... 13
4.1 Filter Substrate Dispersion ... 13
4.2 Shift of the Boresight Position ... 13
5 Temperature Effect on the Boresight Position ... 17
6 Validation of Distortion and Boresight Correction ... 19
7 Pixel Size in Distorted Images ... 21
8 Resampling ... 22
9 Calibration files used by OsiCalliope ... 25
Appendix A. List of images ... 26

List of Figures

Figure 1 Left: NAC distortion correction residual map. Right: WAC distortion correction residual map. Both images are displayed in the standard Rosetta orientation, with CCD pixel coordinates displayed. ... 12

Figure 2: Central ray distance from the optical axis at the edge of the field of view (image height) variation due to wavelength dependent filter dispersion ... 13

Figure 3 X (left) and Y (right) components of the boresight shift as function of ADC temperature for NAC in NAC CCD pixel coordinates ... 17

Figure 4 X (left) and Y (right) components of the boresight shift as function of ADC temperature for WAC in WAC CCD pixel coordinates. ... 17

Figure 5 Residuals of the Vega position on NAC (left) and WAC (right) CCD with different levels of correction applied. Details in the text. ... 20

Figure 6: For a square grid (blue) in level 1 or 2 (CODMAC L2 or L3), the true shape of a pixel in the level 3 (CODMAC L4) frame has an irregular shape, approximated here with four-point polygons (orange) for NAC (left) and WAC (right). Images are in CCD coordinates. 21

Figure 7 Test pattern for verification of radiometric accuracy after resampling. 22

Figure 8 Intensity of test crosses after distortion correction. 23

List of Tables

Table 1: Coefficients for geometric distortion correction. 10

Table 2: Images used for validation of the distortion correction parameters. 11

Table 3: Star map fit results of selected images. The image number in the first column corresponds to the image number in Table 2. 12

Table 4: Vega calibration sequences used for the calculation of the filter dependent boresight shift. 14

Table 5: Boresight shift (in CCD coordinates) of the WAC filters relative to filter F12. 15

Table 6: Boresight shift (in CCD coordinates) of the NAC filters relative to filter F22. 16

Table 7 Coefficients of the linear fit and reference temperature for NAC and WAC. 18

Table 8 Images used to calculate the temperature dependent boresight shift 26

1 General aspects

1.1 Scope

This document describes the method, parameters, and validation for correcting the OSIRIS Narrow Angle Camera (NAC) and Wide Angle Camera (WAC) geometric distortion and for maintaining the boresight in the centre of the image frame.

1.2 Introduction

The OSIRIS NAC utilizes a three mirror and the WAC a two mirror anastigmatic off-axis optical system. Both cameras have high transmission over the UV-VIS-NIR spectral bands, and a chromatic aberration free, near diffraction limited performance. However, the asymmetric optical setup introduces an image distortion.

Both cameras are equipped with a set of band-pass filters in the optical path. Material dispersion, manufacturing and mounting tolerances of the filters introduce a boresight shift. Temperature variations of the spacecraft structure and of the camera mounting also introduce a boresight shift. The image distortion and the boresight shift can be corrected by the resampling method described in the following sections.

1.3 Reference Documents

no.	document name	document number, Iss./Rev.
RD1	OSIRIS User Manual	RO-RIS-MPAE-MA-004, D/s
RD2	OSIRIS Calibration Pipeline OsiCalliope	RO-RIS-MPAE-MA-007 OSIRIS_CAL_PIPELINE_V??.PDF
RD3	Acquisition and processing of flat field images for OSIRIS calibration	RO-RIS-MPAE-TN-075 FLATFIELDING_V??.PDF
RD4	Software Interface Specification for OSIRIS Science Products	RO-RIS-MPAE-ID-023 OSIRIS_SIS_V??.PDF

1.4 Acronyms and Abbreviations

ADC	Analog digital converter
ARP	Anti-radiation plate
CCD	Charge coupled device
iFoV	Instantaneous field of view
NAC	Narrow Angle Camera
OSIRIS	Optical, Spectroscopic, and Infrared Remote Imaging System
LUT	Lookup table
MPS	Max Planck Institute for Solar System Research
WAC	Wide Angle Camera

2 Correction of the Image

This section describes the distortion correction of an OSIRIS image. Details on the required parameters and validation of these are provided in the following sections.

The camera distortion was measured over the full field of view using star-field observations. The values were fitted to a two dimensional polynomial of third or fourth order, which is then used for the correction algorithm. Vega calibration images, acquired throughout the mission, are used to determine the boresight shift with respect to the centre of the image.

The resampling is based on the distortion function, converting from

It is important to understand that the computation for the resampling is based on the resampling function (described in Sect. 8) converting from a pair of undistorted coordinates $(x_\mathrm{u}, y_\mathrm{u})$ to a pair of distorted coordinates $(x_\mathrm{d}, y_\mathrm{d})$. The correction algorithm iterates over pixels in the undistorted (level 3; CODMAC L4) image and takes the intensity from associated pixels in the distorted (level 2; CODMAC L3) image.

The conversion from undistorted to distorted pixel coordinates is calculated as follows:

$$
\begin{aligned}
x_\mathrm{d} &= \sum_{i,j} k_x(i,j) \cdot x_\mathrm{u}^i \cdot y_\mathrm{u}^j + \phi_x + \tau_x(T_\mathrm{ADC2}) \\
y_\mathrm{d} &= \sum_{i,j} k_x(i,j) \cdot x_\mathrm{u}^i \cdot y_\mathrm{u}^j + \phi_y + \tau_y(T_\mathrm{ADC2})
\end{aligned}
\qquad \text{Eq. 1}
$$

The coordinates x and y correspond to samples and lines in the image, respectively. The parameters for this equation are computed such that the equation is to be applied in the CCD coordinate frame as defined in [RD4]. The three terms on the right hand side of the equations are from left to right:

- The correction for the geometric distortion (warping), where k_x and k_y are the coefficients of the polynomial fit. Indexes i and j refer to these coefficients (Table 1). The derivation and validation of these coefficients are provided in Sect. 3.
- The shift of the boresight due offsets between band-pass filters. These values ϕ_x and ϕ_y are a constant per filter combination, i.e. not a function of the location $(x_\mathrm{u}, y_\mathrm{u})$. Details are provided in Sect. 4.
- The shift due to a temperature dependant boresight variation. These factors τ_x and τ_y depend on the temperature, where we found one of the two OSIRIS ADC temperatures, T_ADC2, to show a good correlation. Also this term is a translation, which is not a function of the location $(x_\mathrm{u}, y_\mathrm{u})$. Details are provided in Sect. 5.

To obtain the distortion corrected and boresight-shift corrected OSIRIS Level 3 (CODMAC L4) images, the OSIRIS Level 2 (CODMAC L3) images are non-linearly stretched according to the k_x and k_y distortion removal coefficients.

The resampling method since issue 2 of this document is based on a lookup table (LUT), which provides for every level 3 (CODMAC L4) pixel the coordinates and intensity fractions of pixels in the level 2 (CODMAC L3) image contributing to this pixel. Details on the generation of this LUT and the earlier resampling algorithm are provided in Sect. 7.

Note: For a possible scientific application of measuring coordinates of a feature in distorted level 2 (CODMAC L3) images and converting them into undistorted coordinates, Eq. 1 needs to be inverted. A practical way would be a numerical, iterative approach.

3 Distortion Correction

3.1 Distortion Correction Parameters

The distortion correction parameters were derived using ground calibration and in-flight calibration sequences. The current NAC distortion correction parameters were obtained by fitting early mission distortion measurements stored in a PDS float image format on 2014-10-20. The result was validated using star fields with a residual error of less than 0.2 pixels over the full field of view (Table 3). The WAC distortion correction parameters were reviewed and modified in December 2019 to achieve a better correction. The new WAC distortion correction has less than 1 pixel error over the full field of view (Table 3).

The distortion coefficients for NAC and WAC as to be used in Eq. 1 are provided in Table 1.

3.2 Distortion Correction Reference Point

In October 2019, the distortion parameters were updated to ensure that the physical centre coordinate of the CCD (i.e., the point between the four central pixels) is kept in the same position after the distortion correction is applied.

Table 1: Coefficients for geometric distortion correction.

index		NAC			WAC		
i	*j*	*Poly3*	k_x	k_y	*Poly4*	k_x	k_y
0	0	PAR00	-1.00995600E+01	3.6246000E+00	PAR00	7.857796000E+01	-2.068228000E+01
0	1	PAR01	9.06443000E-04	9.97063000E-01	PAR01	-4.307429000E-02	1.008787140E+00
0	2	PAR02	-5.26902000E-07	-5.93490000E-07	PAR02	2.133265700E-05	1.633132000E-05
0	3	PAR03	-3.32516000E-12	1.99967000E-10	PAR03	8.358309878E-10	-5.311250000E-09
0	4		0.0	0.0	PAR04	-2.307480000E-13	1.614360000E-15
1	0	PAR04	1.01413000E+00	3.21866000E-03	PAR05	9.098868230E-01	-1.122941600E-02
1	1	PAR05	-2.39320000E-07	-3.38901000E-06	PAR06	9.782050000E-06	1.259812000E-05
1	2	PAR06	1.19823000E-10	1.88602000E-12	PAR07	-4.924862000E-09	-1.214809000E-09
1	3	PAR07	-2.01772000E-16	-1.95971000E-17	PAR08	1.285400493E-13	2.451650000E-13
1	4		0.0	0.0	PAR09	0.0	0.0
2	0	PAR08	-4.71201000E-06	-6.41550000E-08	PAR10	3.268638400E-05	3.683580000E-06
2	1	PAR09	8.98608000E-12	1.16434000E-10	PAR11	2.110730000E-10	-5.716986000E-09
2	2	PAR10	-7.17827000E-16	-1.12755000E-16	PAR12	-1.082950000E-13	1.527870000E-13
2	3	PAR11	2.23917000E-19	3.01745000E-20	PAR13	0.0	0.0
2	4		0.0	0.0	PAR14	0.0	0.0
3	0	PAR12	2.91214000E-10	-1.06652000E-11	PAR15	-4.46203600E-09	1.210383200E-09
3	1	PAR13	-1.94627000E-16	-4.15382000E-17	PAR16	-4.100030000E-14	8.519180000E-14
3	2	PAR14	2.20615000E-19	3.98303000E-20	PAR17	0.0	0.0
3	3	PAR15	-6.87882000E-23	-1.09102000E-23	PAR18	0.0	0.0
3	4		0.0	0.0	PAR19	0.0	0.0
4	0		0.0	0.0	PAR20	-1.09946000E-13	-3.160610000E-13
4	1		0.0	0.0	PAR21	0.0	0.0
4	2		0.0	0.0	PAR22	0.0	0.0
4	3		0.0	0.0	PAR23	0.0	0.0
4	4		0.0	0.0	PAR24	0.0	0.0

3.3 Distortion Correction Parameters Validation

The distortion correction parameters were validated using in-flight calibration imaging sequences, and star position fitting. The calculations used the images listed in Table 2, and the Tycho2 star catalogue astrometric data.

Table 2: Images used for validation of the distortion correction parameters.

#	Image ID	Activity Name
1	NAC_2014-03-24T03.07.57.548Z_ID30_1251276900_F22	STP001_ONIT_1
2	NAC_2014-05-11T03.46.11.207Z_ID30_1397549000_F22	STP003_CALIB_FIELD_NAC
3	NAC_2014-05-11T03.44.48.561Z_ID30_1397549000_F24	STP003_CALIB_FIELD_NAC
4	NAC_2014-06-01T11.20.54.559Z_ID30_1397549900_F22	STP004_ONIT_021
5	WAC_2014-03-20T01.14.53.738Z_ID30_1251276000_F12	STP001_WAC_Commissioning
6	WAC_2014-05-11T06.00.38.431Z_ID30_1397549000_F12	STP003_CALIB_FIELD_WAC
7	WAC_2015-09-11T15.10.52.843Z_ID30_1397549000_F12	STP073_GRAIN_TRACK_003

3.3.1 Calculation Method

- The average (A_{pix}) and the standard deviation (S_{pix}) of the pixel intensities were calculated for the full area of the OSIRIS level 3 (CODMAC L4) images.
- The image area was scanned for high intensity, small size, and symmetrical features.
- 2D Gaussian fit was applied on the 15 x 15 pixel area surrounding the highest intensity pixel of the feature for point spread function (PSF) estimation.
- If the standard deviation parameter of the fit in both direction was < 2.2 and the maximum intensity was $> (A_{\mathrm{pix}} + 3S_{\mathrm{pix}})$, the feature was considered a star and the parameters were recorded.
- Star positions of the imaged field of view were extracted from the catalogue, corrected for proper motion.
- The angular positions were projected onto the camera image plane by gnomonic projection using the camera parameters.
- The matching star and detected PSF positions were paired. Detected star positions with no matching catalogue stars were ignored (possible noise, cosmics, etc).
- The camera pointing parameters (Right Ascension, Declination, North Azimuth and camera focus) were optimized to result the smallest deviation of the positions.
- The average and the maximum of the position errors were calculated.

3.3.2 Validation Results

The result of the distortion correction parameters validation is summarized in Table 3.

Between 72 and 231 stars were detected per image, being evenly distributed over the field of view. An outcome of the star fitting is the PSF, which 1-sigma value from a Gaussian fit was found to be approximately ± 1.0 pixel for both cameras. This is slightly larger than described in the OSIRIS ground calibration [RD1].

The focal length is treated as a free parameter in this validation and perfectly matches the focal length the distortion correction was set to. The design values for the OSIRIS Level 3 (CODMAC L4) products are 717.322 mm for the NAC (L. Jorda, pers. comm.) and 135.68 mm for the WAC (V. Da Deppo, pers. comm.). This is consistent with the information in the OSIRIS instrument kernels of the Rosetta Spice set (ROS_OSIRIS_V14.TI and later).

Table 3: Star map fit results of selected images. The image number in the first column corresponds to the image number in Table 2.

#	Camera	Number of Stars	Error		Calculated pointing			
			Maximum [pix]	Average [pix]	Right Ascension [°]	Declination [°]	Celestial North [°]	Focal Length [mm]
1	NAC	109	0.57	0.13	4.3255	-0.2311	2.1439	717.28
2	NAC	82	0.63	0.16	4.3431	-0.2444	5.2378	717.32
3	NAC	72	0.64	0.17	4.3431	-0.2444	5.2379	717.31
4	NAC	108	0.57	0.13	4.3665	-0.2745	5.1932	717.29
5	WAC	293	0.72	0.33	247.5072	-13.0973	-13.0973	135.678
6	WAC	373	0.86	0.30	248.4903	-13.8681	13.8681	135.678
7	WAC	129	0.73	0.21	82.3033	-0.8758	2511.734	135.678

The remaining distortion-correction residuals are well below 1 pixel for both NAC and WAC. Typical errors for the NAC are below 0.2 pixels and for the WAC below 0.3 pixels (see Table 3), which is smaller than the PSF (~1 pixel) described above. It should be noted that the displayed colours in Figure 1 represent *absolute numbers* of known *directed errors*.

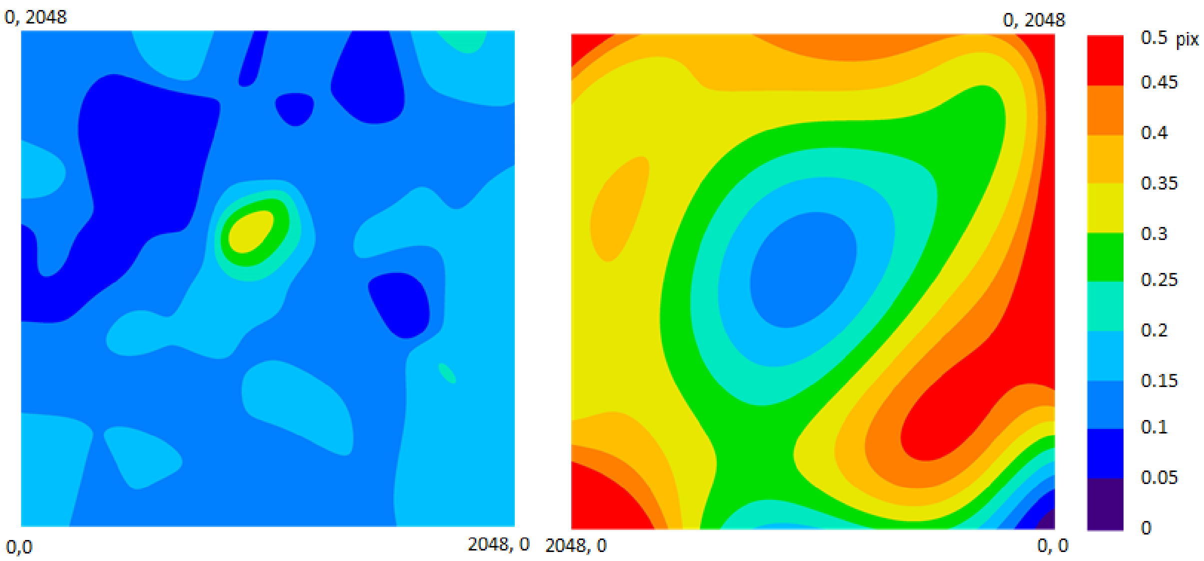

Figure 1 Left: NAC distortion correction residual map. Right: WAC distortion correction residual map. Both images are displayed in the standard Rosetta orientation, with CCD pixel coordinates displayed.

4 Effect of the Band-Pass Filters on Boresight Position

The camera distortion and position of the boresight in the image are also affected by the band-pass filter in the optical path. Two major effects should be considered:

- The dispersion of the substrate material causes a slight magnification change by the transmitted wavelength
- The manufacturing and mounting tolerances of the filters can cause a small shift in the image position

4.1 Filter Substrate Dispersion

Both cameras are mirror systems and the only refractive components are the anti-radiation plate (ARP) and filters. Those components have plane surfaces, with a 10’ wedge angle, so the expected effect is small. The magnification variation was modelled by raytracing calculations: the meridional image size (the distance between the image center and the first column) was calculated as a function of the wavelength.

The NAC exhibited no significant change of the meridional image size vs. wavelength. The WAC showed less than half a pixel in the 300 – 700 nm bands, and about a pixel below 300 nm.

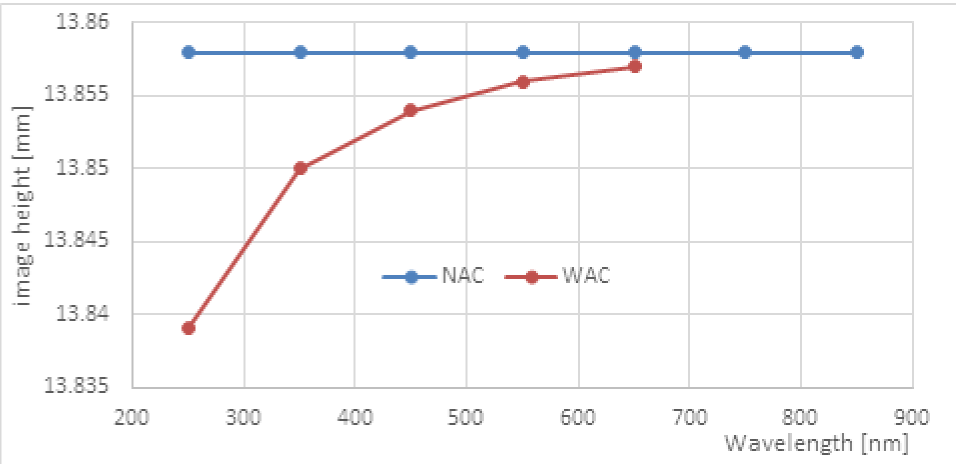

Figure 2: Central ray distance from the optical axis at the edge of the field of view (image height) variation due to wavelength dependent filter dispersion

4.2 Shift of the Boresight Position

The shift of the boresight position with respect to the image centre is due to the manufacturing and mounting tolerance of the filters of both cameras, NAC and WAC. In addition, as seen in Sec. 4.1, the WAC substrate dispersion is also dependent on the wavelength of the filter band-pass.

The filter dependant boresight shift was measured on Vega calibration sequences acquired during the entire mission (Table 4). During these observations, Vega was imaged close to the optical axis, and sequences of images were acquired with different filters. The star position was determined in each image by PSF fitting. NAC F22 and WAC F12 were selected as reference filters. For each image, the shift of the determined Vega position with respect to the position in the reference filter was calculated in CCD coordinates. The average (over the entire mission) shift per filter represents the shift of the boresight position with respect to the image centre. The boresight shift parameters (ϕ_x, ϕ_y) per filter are listed in Table 5 and Table 6.

Table 4: Vega calibration sequences used for the calculation of the filter dependent boresight shift.

Calibration sequence	Start time	End time
MARS_2007-2	2007-02-23T12:38:04	2007-02-23T12:54:07
EAR_2007-11	2007-11-11T21:48:00	2007-11-11T21:54:04
AST1	2008-09-03T18:03:42	2008-09-03T18:25:35
EAR3-2009-11	2009-11-10T20:31:29	2009-11-10T20:41:55
CR5_2010_5	2010-05-01T03:51:56	2010-05-01T03:57:10
AST2	2010-07-12T00:33:41	2010-07-12T00:55:31
STP003_CALIB_STARS_001	2014-05-18T08:59:18	2014-05-18T09:15:11
STP035_VEGA_001	2014-12-22T13:23:52	2014-12-22T13:28:35
STP037_VEGA_002	2015-01-05T14:03:52	2015-01-05T14:08:36
STP039_VEGA_001	2015-01-20T15:12:21	2015-01-20T15:17:05
STP043_VEGA_001	2015-02-11T18:14:34	2015-02-11T18:19:17
STP069_VEGA_001	2015-08-14T14:49:27	2015-08-14T14:53:31
STP075_VEGA_001	2015-09-28T04:36:03	2015-09-28T04:40:12
STP083_VEGA_001	2015-11-24T15:05:34	2015-11-24T15:09:55
STP085_VEGA_002	2015-12-08T21:18:44	2015-12-08T21:23:05
STP089_VEGA_001	2015-12-31T20:29:34	2015-12-31T20:31:17
STP094_VEGA_001	2016-02-08T14:34:52	2016-02-08T14:44:24
STP098_VEGA_001	2016-03-08T20:44:07	2016-03-08T20:55:15
STP100_VEGA_001	2016-03-21T14:34:37	2016-03-21T14:45:45
STP107_VEGA_001	2016-05-10T20:44:04	2016-05-10T20:55:13
STP114_VEGA_001	2016-06-28T14:02:30	2016-06-28T14:04:53
STP119_VEGA_001	2016-08-02T16:35:37	2016-08-02T16:38:01

Table 5: Boresight shift (in CCD coordinates) of the WAC filters relative to filter F12.

Filter	ϕ_x (pix)	ϕ_y (pix)	Standard deviation of ϕ_x (pix)	Standard deviation of ϕ_y (pix)
12	0.00	0.00	-	-
13	-0.30	0.03	0.21	0.16
14	-0.29	-0.08	0.24	0.20
15	-0.50	0.08	0.18	0.08
16	-0.47	0.01	0.33	0.16
17	-0.40	-0.28	0.29	0.17
18	-0.41	-0.07	0.17	0.12
21	-2.37	-0.04	0.15	0.07
31	-2.02	0.00	0.12	0.04
41	-1.97	0.25	0.35	0.26
51	-1.81	-0.14	0.31	0.17
61	-1.52	-0.15	0.17	0.16
71	-1.77	0.05	0.10	0.14
81	-2.40	0.10	0.37	0.11

Table 6: Boresight shift (in CCD coordinates) of the NAC filters relative to filter F22.

Filter	ϕ_x (pix)	ϕ_y (pix)	Standard deviation of ϕ_x (pix)	Standard deviation of ϕ_y (pix)
15	4.16	-1.29	1.63	0.91
16	3.88	-1.11	1.80	0.87
22	0.00	0.00	0.00	0.00
23	-1.03	-0.36	1.30	0.71
24	-0.44	-0.64	1.60	0.72
26	-0.85	-0.45	-	-
27	-0.64	-0.12	1.96	0.78
28	-0.80	-0.42	1.75	0.76
32	4.13	-0.57	1.55	0.86
33	3.28	-0.83	1.60	0.74
35	3.86	-1.27	-	-
36	3.61	-1.16	-	-
37	3.40	-0.41	-	-
38	3.51	-0.93	1.46	0.67
41	4.49	-1.06	1.84	1.02
51	4.40	-1.14	1.92	1.03
58	-1.14	-0.79	1.62	0.76
61	3.57	-1.01	1.66	0.93
71	3.74	-0.98	1.38	0.72
81	10.08	-1.40	1.06	0.78
82	5.33	-0.68	0.81	0.50
83	4.50	-1.12	1.28	0.70
84	5.32	-1.29	1.37	0.74
86	5.29	-1.23	0.81	0.50
87	4.68	-0.72	1.95	0.69
88	4.82	-1.18	1.68	0.68

5 Temperature Effect on the Boresight Position

The position of the boresight in the image is affected by the actual temperature of the spacecraft structure and of the camera mounting. Vega, Zeta Cas and star field images, acquired during the entire mission at different temperatures (see Table 8), were used to calculate the shift of the boresight with respect to the centre of the image. As temperature proxy the ADC2 temperature (provided in the image header) was used. Those temperatures were cross checked against S/C housekeeping of deck temperatures in NAC and WAC vicinity (NTSA0007 and NTSA0008, respectively) and did not show qualitative differences. In each image the position of the star is measured through PSF fitting. The position of the central pixel is what we refer to as measured Vega position. The difference between the measured Vega position and the expected one (based on star catalogues) is computed for each image and displayed as function of temperature in Figure 3 (for NAC) and in Figure 4 (for WAC).

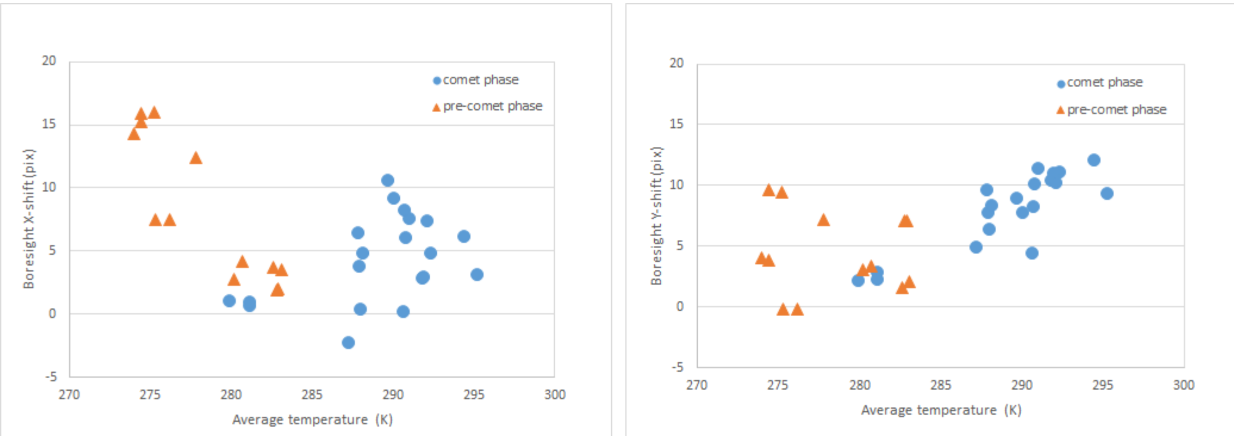

Figure 3 X (left) and Y (right) components of the boresight shift as function of ADC temperature for NAC in NAC CCD pixel coordinates.

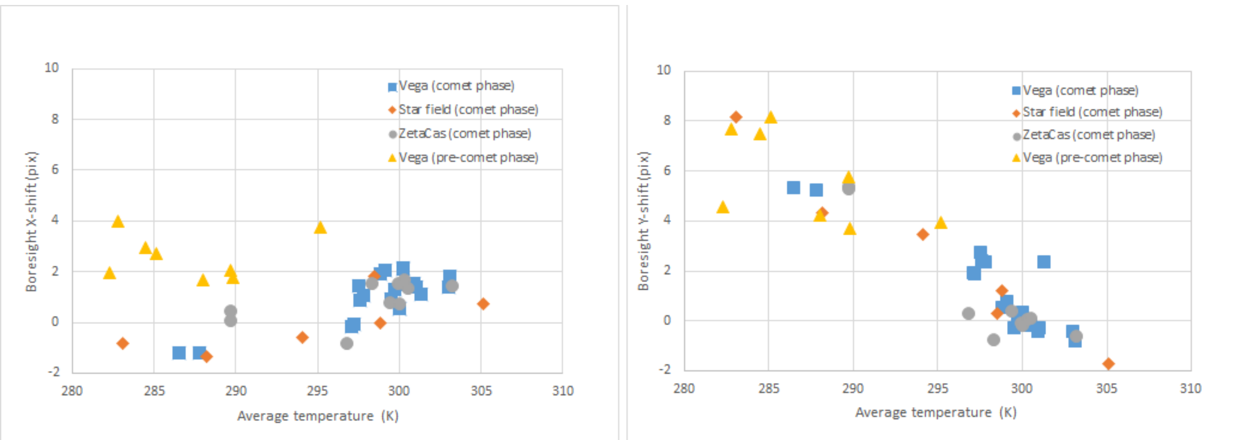

Figure 4 X (left) and Y (right) components of the boresight shift as function of ADC temperature for WAC in WAC CCD pixel coordinates.

The temperature dependent boresight shift (x- and y-component) is calculated using a linear interpolation of the (*expected – measured*) Vega positions as function of temperature:

$$\tau_x(T_{\mathrm{ADC2}}) = A_x \cdot (T_{\mathrm{ADC2}} - T_0) + B_x$$
$$\tau_y(T_{\mathrm{ADC2}}) = A_y \cdot (T_{\mathrm{ADC2}} - T_0) + B_y \quad , \qquad \text{Eq. 2}$$

where T_{ADC2} is one of the two OSIRIS ADC temperatures. The reference temperature T_0 is chosen such that the curve crosses the zero at the reference temperature. The coefficients A and B of the linear fits and reference temperatures for NAC and WAC are listed in Table 7.

Table 7 Coefficients of the linear fit and reference temperature for NAC and WAC.

PARAMETER	CAMERA	
	NAC	WAC
A_x (pix/K)	0.297	0.150
B_x (pix)	4.54	1.17
A_y (pix/K)	0.583	-0.421
B_y (pix)	8.67	0.48
T_0 (K)	290	300

The constant part of the linear fit (i.e., B_x and B_y) is used to correct the absolute boresight position in the SPICE frame kernel, i.e., obtaining an average residual boresight shift in x and y direction centred on zero. Thus, the temperature dependent boresight correction that is applied to each image by OsiCalliope is:

$$\tau_x(T_{\mathrm{ADC2}}) = A_x \cdot (T_{\mathrm{ADC2}} - T_0)$$
$$\tau_y(T_{\mathrm{ADC2}}) = A_y \cdot (T_{\mathrm{ADC2}} - T_0) \qquad \text{Eq. 3}$$

The linear coefficients (i.e., A_x and A_y) reduce the dispersion of the boresight residuals around the zero position.

6 Validation of Distortion and Boresight Correction

We used all the Vega sequences acquired during the comet phase and several acquired in the pre-comet phase to verify the effects (in terms of boresight residual) of all components of the distortion correction and boresight shift correction applied to the data.

Figure 5 shows the residual of the Vega position on the NAC (left) and WAC (right) CCD.

Top: Vega images calibrated using the original geometric distortion parameters, with no filter dependent boresight correction ($\phi_x = \phi_y = 0$) and temperature dependent boresight correction ($\tau_x = \tau_y = 0$). Theoretical values are calculated using the frame kernel ROS_V35.TF.

Centre: Vega images calibrated using the updated geometric distortion correction parameters (orange), further corrected for filter dependent boresight shift (violet) and temperature dependent boresight shift (pink). Theoretical values are the same as in the top panel. Residuals are reduced.

Bottom: Same as the central panel but with residuals calculated against theoretical values calculated using updated absolute boresight from frame kernel ROS_V36.TF (green). The final residuals are centred around $(0, 0)$

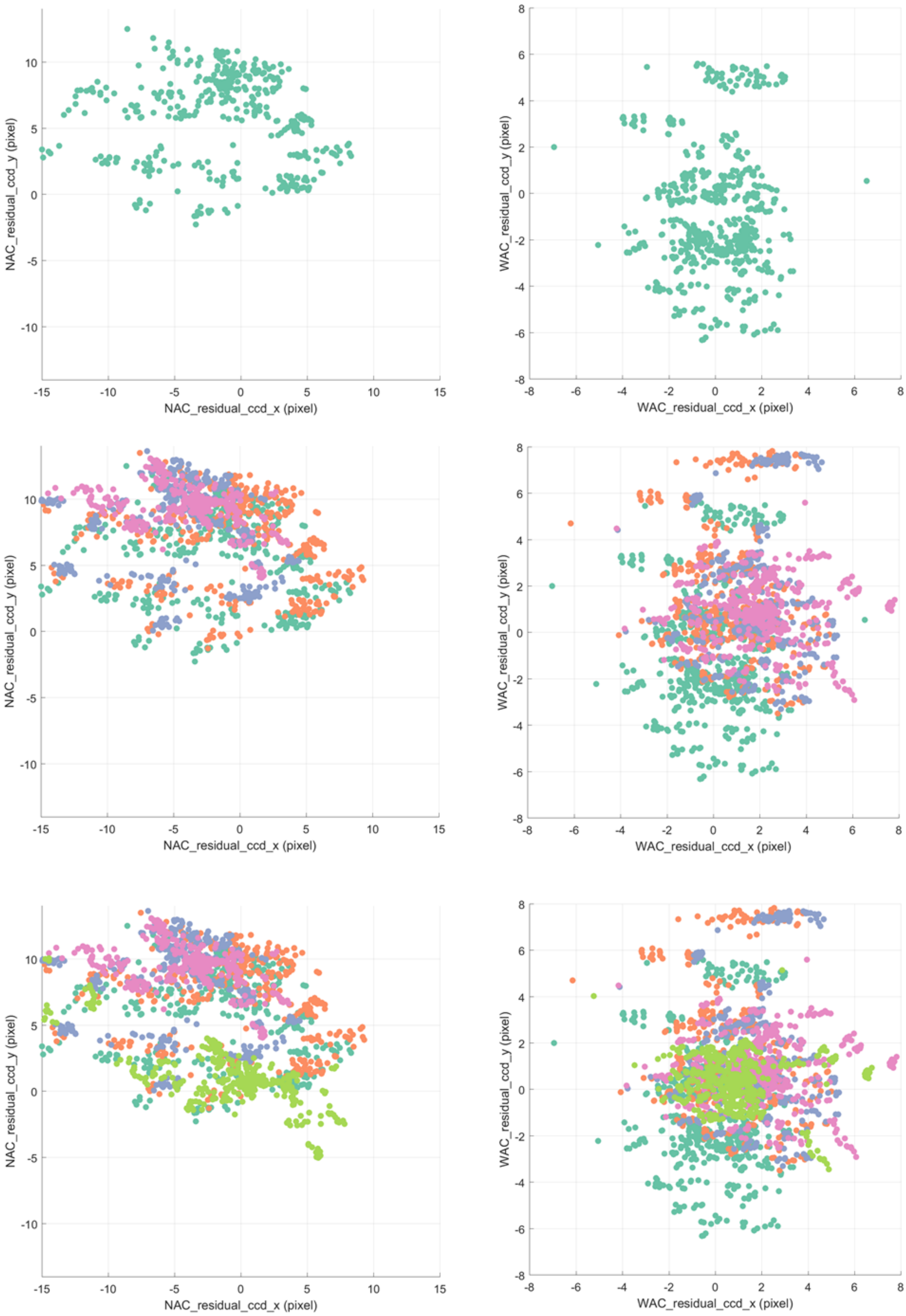

Figure 5 Residuals of the Vega position on NAC (left) and WAC (right) CCD with different levels of correction applied. Details in the text.

7 Pixel Size in Distorted Images

Due to the OSIRIS off-axis design, the focal length (thus iFoV) is not constant over the field. We are here interested in the pixel size – the solid angle or squared iFoV of a pixel – from which a pixel collects the light. As undistorted images have a constant pixel size over the field, the area of a square pixel in a level 2 (CODMAC L3) image transformed into level 3 (CODMAC L4) corresponds to the pixel size of this level 2 (CODMAC L3) pixel.

To compute this, we approximated each level 2 (CODMAC L3) pixel with a 4-point polygon and converted the four corner coordinates into the level 3 (CODMAC L4) frame using an inversion of the distortion equation (Eq. 1). The area of this non-rectangular polygon provides the pixel size relative to the level 3 (CODMAC L4) pixel size.

This is visualised in Figure 6 (NAC left, WAC right). For the sake of visibility, each square represents 64x64 pixels. The blue raster represents the level 2 (CODMAC L3) grid of pixels with square shapes. Inverting Eq. 1, every node is converted into the level 3 (CODMAC L4) frame, which results in a displacement but also a change in shape and size (orange raster). This can be best seen for the pixel (0, 0) in the WAC frame, which is shifted towards the left and slightly down. The reasonable approximation by four points implies that the polygon has four straight lines, which are formally curved. The sizes of the orange polygons determine the relative pixel sizes of the corresponding blue polygons.

The pixel size for level 2 (CODMAC L3) pixels in units of the undistorted pixel size is provided as a pre-calculated image file under the name [*CAMERA*]_FM_PIXEL_SIZE_V[*VERSION*].IMG.

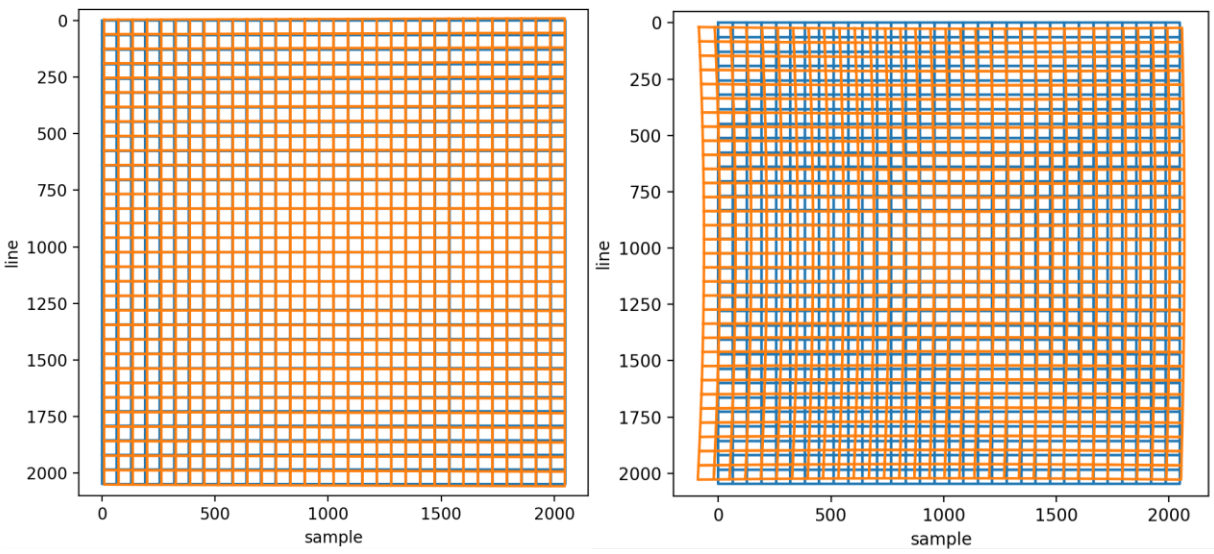

Figure 6: For a square grid (blue) in level 1 or 2 (CODMAC L2 or L3), the true shape of a pixel in the level 3 (CODMAC L4) frame has an irregular shape, approximated here with four-point polygons (orange) for NAC (left) and WAC (right). Images are in CCD coordinates.

8 Resampling

Resampling the image means that the intensity of each pixel in the level 3 (CODMAC L4) is taken from a number of pixels in the level 2 (CODMAC L3) image. The location of these pixels is given by Eq. 1, but the exact choice in terms of number of involved level 2 (CODMAC L3) pixels and their weighting is a choice of the specific resampling algorithm.

The resampling of the image before issue 2 of this document was based on an area weighted bi-linear algorithm. This means that each level 3 (CODMAC L4) pixel receives the intensity from exactly 4 level 2 (CODMAC L3) pixels, which are weighted according to the distance to the centre of the level 3 (CODMAC L4) pixel converted to level 2 (CODMAC L3) using Eq. 1.

The analysis of star calibration images revealed that this resampling method causes radiometric uncertainties in case of point sources and fast changing intensity regions. This error depends on pixel location and can be as large as a few percent. The issue is due to an aliasing effect resulting from the fixed pitch resampling of a variable size raster (the undistorted image is unevenly stretched with respect of the original).

The effect was demonstrated by undistorting a test image with cross pattern of 5 pixels with 10,000 DN each (50,000 DN in total) spread over the field (see Figure 7).

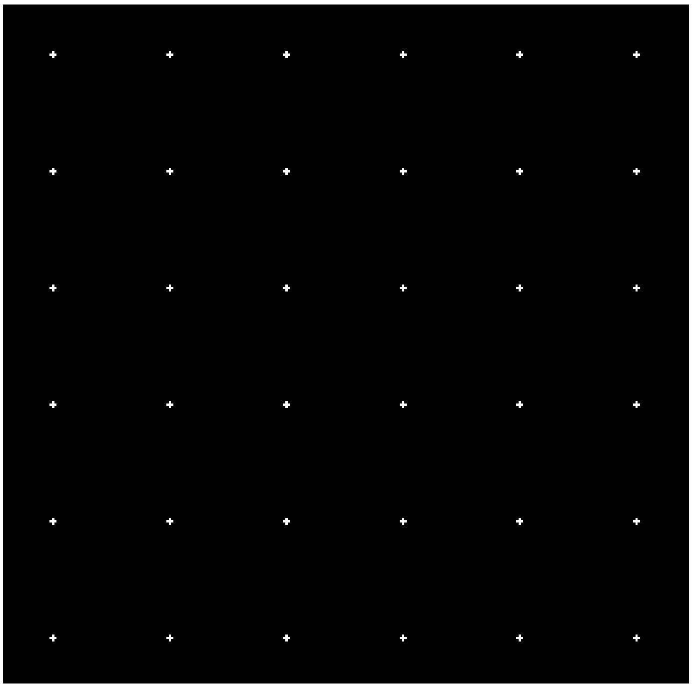

Figure 7 Test pattern for verification of radiometric accuracy after resampling.

This test image was resampled using (a) the former bi-linear algorithm and (b) an improved pixel-shape aware method described below. The resulting aperture photometry of the artificial stars are calculated in the undistorted image and presented in Figure 8.

The blue curve represents the integrated intensity per cross from the bi-linear algorithm (old), the orange curve is the integrated intensity from the iFoV aware algorithm (new). First, it is evident that the intensity changed from 50,000 DN to an intensity, which is a function of the sample position x. This is the consequence of the variation of the changing iFoV in distorted images. The representation of the cross in distortion corrected images becomes larger. This effect is described in [RD3] and a desired consequence of the flat fielding.

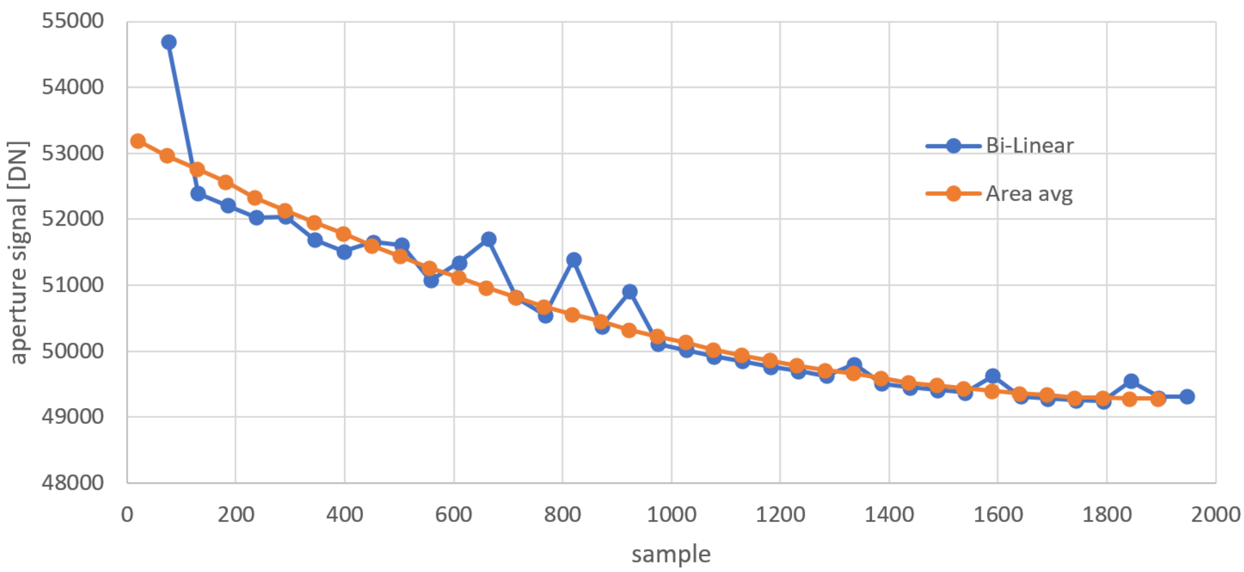

Figure 8 Intensity of test crosses after distortion correction.

It can be shown that the orange curve (iFoV aware resampling) follows the pixel-size factor provided in [RD3] to a precision of 0.1 %. This means that the photometric error after distortion correction shows statistical noise in the order of 0.1%. In contrast to that, the blue curve (bi-linear resampling, old method) shows a substantial scatter around the orange curve. The majority of pixels are below the orange curve (missing intensity) and some values are above the correct intensity. For a sufficiently large number of points, the average of the blue curve approaches the orange curves. However, all individual pixels have an inaccurate photometric intensity with the old bi-linear resampling method.

In order to avoid the above effect, a new iFoV aware resampling method was developed. The method uses the following steps for each level 3 (CODMAC L4) pixel:

- The 4 corners of a level 3 (CODMAC L4) pixel are converted into the level 2 (CODMAC L3) coordinate system using Eq. 1. These correspond to a 4-corner polygon.
- The intersection area of each level 2 (CODMAC L3) pixel with this polygon is calculated.
- The intensity of each intersecting pixel is weighted by its intersection area, normalized by the total polygon area.
- The weighted intensities are summed up, the result is the undistorted pixel intensity.

To speed up the calculations, the undistorted pixel area segments are pre-computed and stored in a lookup table (LUT).

The new resampling algorithm was introduced in issue 2 of this document and used since version 2.29 of OsiCalliope (the version is documented in each image header).

Due to the binary nature of the image quality map [RD2], this is resampled differently. A pixel shall be flagged with a quality bit value in level 3 (CODMAC L4) image whenever any pixel from level 2 (CODMAC L3) that contributed to it is flagged. Therefore each pixel is calculated as a binary OR of the quality flags for each of the original pixels which contribute to the resampled pixel.

9 Calibration files used by OsiCalliope

The calibration files used by OsiCalliope [RD2] to calibrate OSIRIS images are:

- NAC_FM_DISTORTION_V02.TXT
- WAC_FM_DISTORTION_V02.TXT
- NAC_FM_PIXEL_SIZE_V01.IMG (since issue 2)
- WAC_FM_PIXEL_SIZE_V01.IMG (since issue 2)

Previous versions:

- NAC_FM_DISTORTION.LBL
  (obsolete, same values as NAC_FM_DISTORTION_V01.TXT)
- WAC_FM_DISTORTION.LBL
  (obsolete, same values as WAC_FM_DISTORTION_V01.TXT)

Appendix A. List of images

Table 8 Images used to calculate the temperature dependent boresight shift

MISSION PHASE			FILENAME	TARGET	T_{ADC2} (deg)	T_{ADC1} (deg)
COMMISSIONING	CVP2	2004_09	WAC_2004-09-24T13.44.03.100Z _ID10_3610015002_F12	VEGA	284.8	283.3
MARS	MARS	2007_02	WAC_2007-02-23T12.50.06.951Z _ID10_0050041000_F12	VEGA	289.7	288.4
EARTH	EAR2	2007_09	WAC_2007-09-13T05.39.03.969Z _ID10_0000078000_F12	VEGA	288	287.8
EARTH	EAR2	2007_09	WAC_2007-09-13T06.01.03.954Z _ID10_0000118000_F12	VEGA	289.8	289.5
EARTH	EAR2	2007_11	WAC_2007-11-11T21.50.03.989Z _ID10_0115015000_F12	VEGA	295.2	293.8
STEINS	AST1	2008_09	WAC_2008-09-03T18.19.22.030Z _ID10_0167036000_F12	VEGA	285.1	284.3
EARTH	EAR3	2009_11	WAC_2009-11-10T20.37.55.576Z _ID10_1251276000_F12	VEGA	282.8	281.4
CRUISE	CR5	2010_05	WAC_2010-05-01T03.53.09.106Z _ID10_1251276006_F12	VEGA	282.3	280.8
LUTETIA	AST2	2010_07	WAC_2010-07-12T00.49.18.835Z _ID10_1251276000_F12	VEGA	284.5	283.3
67P	MTP003	STP003_CALIB_STARS_001	WAC_2014-05-18T09.02.37.224Z _ID10_1397549000_F12	VEGA	286.5	286.5
67P	MTP003	STP003_CALIB_STARS_001	WAC_2014-05-18T09.11.19.133Z _ID10_1397549000_F12	VEGA	287.8	287.2
67P	MTP011	STP035_VEGA_001	WAC_2014-12-22T13.25.00.393Z _ID10_1397549006_F12	VEGA	297.5	296.2
67P	MTP012	STP039_VEGA_001	WAC_2015-01-20T15.13.38.380Z _ID10_1397549007_F21	VEGA	297.6	296.3
67P	MTP013P	STP043_VEGA_001	WAC_2015-02-11T18.15.42.148Z _ID10_1397549006_F12	VEGA	297.8	296.5
67P	MTP018P	STP066_VEGA_002	WAC_2015-07-24T20.03.29.957Z _ID10_1397549006_F12	VEGA	301.3	299.9
67P	MTP019P	STP069_VEGA_001	WAC_2015-08-14T14.50.36.577Z _ID10_1397549006_F12	VEGA	303.1	301.8
67P	MTP021P	STP075_VEGA_001	WAC_2015-09-28T04.37.13.504Z _ID10_1397549006_F12	VEGA	299.1	297.8
67P	MTP023P	STP083_VEGA_001	WAC_2015-11-24T15.06.53.596Z _ID10_1397549006_F12	VEGA	299.5	299.1

67P	MTP023P	STP085_VEGA_002	WAC_2015-12-08T21.20.03.008Z _ID10_1397549006_F12	VEGA	298.8	298.3
67P	MTP024P	STP089_VEGA_001	WAC_2015-12-31T20.30.30.312Z _ID10_1397549006_F12	VEGA	303	302
67P	MTP025P	STP094_VEGA_001	WAC_2016-02-08T14.35.02.257Z _ID10_1397549001_F12	VEGA	299.7	298.4
67P	MTP026P	STP098_VEGA_001	WAC_2016-03-08T20.44.08.060Z _ID10_1397549000_F12	VEGA	300.4	299.1
67P	MTP026P	STP098_VEGA_001	WAC_2016-03-08T20.44.29.178Z _ID10_1397549001_F12	VEGA	300.5	299.1
67P	MTP027P	STP100_VEGA_001	WAC_2016-03-21T14.34.37.703Z _ID10_1397549000_F12	VEGA	300.2	298.9
67P	MTP027P	STP100_VEGA_001	WAC_2016-03-21T14.35.00.503Z _ID10_1397549001_F12	VEGA	300.2	298.9
67P	MTP029P	STP107_VEGA_001	WAC_2016-05-10T20.44.04.776Z _ID10_1397549000_F12	VEGA	301	299.6
67P	MTP029P	STP107_VEGA_001	WAC_2016-05-10T20.44.27.762Z _ID10_1397549001_F12	VEGA	300.9	299.6
67P	MTP030P	STP114_VEGA_001	WAC_2016-06-28T14.02.27.832Z _ID10_1397549000_F12	VEGA	300	298.7
67P	MTP030P	STP114_VEGA_001	WAC_2016-06-28T14.02.47.898Z _ID10_1397549001_F12	VEGA	300	298.7
67P	MTP032P	STP119_VEGA_001	WAC_2016-08-02T16.35.36.784Z _ID10_1397549000_F12	VEGA	297.1	295.9
67P	MTP032P	STP119_VEGA_001	WAC_2016-08-02T16.35.56.661Z _ID10_1397549001_F12	VEGA	297.2	295.8
67P	MTP003	STP003_ALICE_X_XAL_003	WAC_2014-05-13T20.51.45.736Z _ID10_1397549000_F12	ZETA CAS	289.7	288.5
67P	MTP003	STP003_ALICE_X_XAL_001	WAC_2014-05-13T20.19.46.432Z _ID10_1397549000_F12	ZETA CAS	289.7	288.5
67P	MTP019P	STP069_ZETA_CAS_002	WAC_2015-08-18T20.18.52.260Z _ID10_1397549005_F13	ZETA CAS	303.2	302.3
67P	MTP021P	STP075_ZETA_CAS_001	WAC_2015-09-25T15.35.24.637Z _ID10_1397549000_F13	ZETA CAS	299.9	298.5
67P	MTP023P	STP083_ZETA_CAS_001	WAC_2015-11-24T20.44.09.951Z _ID10_1397549000_F13	ZETA CAS	298.3	298.6
67P	MTP024P	STP088_ZETA_CAS_001	WAC_2015-12-25T20.02.17.804Z _ID10_1397549000_F13	ZETA CAS	300	298.7
67P	MTP025P	STP094_ZETA_CAS_002	WAC_2016-02-09T15.05.22.521Z _ID10_1397549250_F13	ZETA CAS	300.3	299
67P	MTP026P	STP098_ZETA_CAS_001	WAC_2016-03-08T15.05.32.466Z _ID10_1397549450_F13	ZETA CAS	300.5	299.2

67P	MTP028P	STP104_ZETA_CAS_001	WAC_2016-04-15T20.02.32.467Z _ID10_1397549750_F13	ZETA CAS	299.4	298.1
67P	MTP030P	STP111_ZETA_CAS_001	WAC_2016-06-03T20.09.34.470Z _ID10_1397549612_F13	ZETA CAS	296.8	296.7
COMMISSIONING	CVP2	2004_09	NAC_2004-09-24T13.33.23.893Z _ID10_3610001002_F82	VEGA	281.5	280.6
MARS	MARS	2007_02	NAC_2007-02-23T12.39.10.980Z _ID10_0050018000_F22	VEGA	282.8	282.2
MARS	MARS	2007_02	NAC_2007-02-23T12.40.15.956Z _ID10_0050024000_F82	VEGA	282.9	282.3
EARTH	EAR2	2007_09	NAC_2007-09-13T05.06.07.951Z _ID10_0000015000_F22	VEGA	280.2	279.4
EARTH	EAR2	2007_09	NAC_2007-09-13T05.07.12.943Z _ID10_0000021000_F82	VEGA	280.7	279.9
EARTH	EAR2	2007_09	NAC_2007-09-13T05.28.07.951Z _ID10_0000055000_F22	VEGA	283.1	283.3
EARTH	EAR2	2007_09	NAC_2007-09-13T05.29.13.932Z _ID10_0000061000_F82	VEGA	282.6	283.2
STEINS	AST1	2008_09	NAC_2008-09-03T18.09.55.929Z _ID10_0167019000_F82	VEGA	277.8	277.3
EARTH	EAR3	2009_11	NAC_2009-11-10T20.32.39.868Z _ID10_1251276000_F22	VEGA	274.4	273.5
EARTH	EAR3	2009_11	NAC_2009-11-10T20.33.53.743Z _ID10_1251276000_F82	VEGA	275.2	274.4
CRUISE	CR5	2010_05	NAC_2010-05-01T03.53.04.985Z _ID10_1251276006_F22	VEGA	275.3	275.1
CRUISE	CR5	2010_05	NAC_2010-05-01T03.54.29.792Z _ID10_1251276000_F82	VEGA	276.2	276
LUTETIA	AST2	2010_07	NAC_2010-07-12T00.36.47.863Z _ID10_1251276000_F22	VEGA	274	274.6
LUTETIA	AST2	2010_07	NAC_2010-07-12T00.39.54.816Z _ID10_1251276000_F82	VEGA	274.4	274.9
67P	MTP001	STP001_NAC _Commissioning	NAC_2014-03-20T23.06.35.558Z _ID10_1251276000_F22	67P	279.1	278.6
67P	MTP003	STP003_CALIB_STARS_001	NAC_2014-05-18T09.00.52.322Z _ID10_1397549000_F22	VEGA	281.1	281.2
67P	MTP003	STP003_CALIB_STARS_001	NAC_2014-05-18T09.01.22.567Z _ID10_1397549000_F82	VEGA	281.1	281.2
67P	MTP003	STP003_CALIB_STARS_001	NAC_2014-05-18T09.09.34.388Z _ID10_1397549000_F22	VEGA	279.9	280.8
67P	MTP011	STP035_VEGA_001	NAC_2014-12-22T13.25.12.252Z _ID10_1397549007_F82	VEGA	287.8	288

67P	MTP011	STP037_VEGA_002	NAC_2015-01-05T14.05.12.500Z_ID10_1397549007_F82	VEGA	288	288.3
67P	MTP012	STP039_VEGA_001	NAC_2015-01-20T15.13.42.406Z_ID10_1397549007_F82	VEGA	287.9	288.1
67P	MTP013P	STP043_VEGA_001	NAC_2015-02-11T18.15.53.878Z_ID10_1397549007_F82	VEGA	288.1	288.3
67P	MTP018P	STP066_VEGA_002	NAC_2015-07-24T20.03.42.306Z_ID10_1397549007_F82	VEGA	292.3	292.5
67P	MTP019P	STP069_VEGA_001	NAC_2015-08-14T14.50.49.022Z_ID10_1397549007_F82	VEGA	294.4	294.6
67P	MTP021P	STP075_VEGA_001	NAC_2015-09-28T04.36.50.285Z_ID10_1397549004_F82	VEGA	289.7	290.1
67P	MTP022P	STP082_VEGA_002	NAC_2015-11-13T15.34.38.614Z_ID10_1397549004_F82	VEGA	291.8	292.2
67P	MTP023P	STP083_VEGA_001	NAC_2015-11-24T15.06.23.612Z_ID10_1397549004_F82	VEGA	291.9	292.4
67P	MTP023P	STP085_VEGA_002	NAC_2015-12-08T21.19.31.054Z_ID10_1397549004_F82	VEGA	291	291.4
67P	MTP024P	STP089_VEGA_001	NAC_2015-12-31T20.30.21.480Z_ID10_1397549004_F82	VEGA	295.2	295.2
67P	MTP025P	STP094_VEGA_001	NAC_2016-02-08T14.35.28.614Z_ID10_1397549004_F82	VEGA	290	290.4
67P	MTP026P	STP098_VEGA_001	NAC_2016-03-08T20.44.55.446Z_ID10_1397549004_F82	VEGA	290.8	291.2
67P	MTP027P	STP100_VEGA_001	NAC_2016-03-21T14.35.23.987Z_ID10_1397549004_F82	VEGA	290.7	291.1
67P	MTP028P	STP104_VEGA_001	NAC_2016-04-19T20.44.54.274Z_ID10_1397549004_F82	VEGA	291	291.4
67P	MTP029P	STP107_VEGA_001	NAC_2016-05-10T20.44.51.323Z_ID10_1397549004_F82	VEGA	292.1	292.5
67P	MTP030P	STP114_VEGA_001	NAC_2016-06-28T14.03.16.615Z_ID10_1397549004_F82	VEGA	290.6	291.1
67P	MTP032P	STP119_VEGA_001	NAC_2016-08-02T16.36.24.586Z_ID10_1397549004_F82	VEGA	287.2	287.7